CONCEPTUAL DESIGN OF A TWO-STAGE-TO-ORBIT VEHICLE

CASE WESTERN RESERVE UNIVERSITY

A conceptual design study of a two-stage-to-orbit vehicle is presented. Three configurations were initially investigated with one configuration selected for further development. The major objective was to place a 20,000-lb payload into a low Earth orbit using a two-stage vehicle. The first stage used air-breathing engines and employed a horizontal takeoff, while the second stage used rocket engines to achieve a 250-n.m. orbit. A two-stage-to-orbit vehicle seems a viable option for the next-generation space shuttle.

INTRODUCTION

The space shuttle system currently in use by NASA uses a conventional method of rocket boost to place a payload in orbit. The space shuttle is essentially a cargo bay assisting in no way on the ascent trajectory. Its advantage comes at the end of its flight as it uses aerodynamic forces to return for a landing and be refurbished and put back into orbit. Another method exists to place a payload in orbit: this method involves using aerodynamic forces to assist in the ascent trajectory. The vehicle can either be flown to orbit directly from a runway using aerodynamic lifting forces as much as practical, or it can be boosted by one or more stages. This vehicle would resemble the X-15 experimental research airplane in overall configuration.

It was decided to use horizontal takeoff for the boost stage of a Two-Stage-to-Orbit vehicle. The horizontal takeoff would use less fuel than a vertical-type liftoff system because the engine would not have to produce enough thrust to support the weight. It could make maximum use of aerodynamic forces for lifting instead of just contributing to the drag of a typical vertical launch system. Two stages were chosen for this vehicle. The first stage was to take advantage of the high specific impulse of air-breathing engines and aerodynamic lift as much as practical. The booster stage would then separate from the orbiter and return to land and be reused. The orbiter would then ascend using the lower specific impulse rocket propulsion, but without the weight of the now-inactive airbreathing engines, associated fuel system, and the inefficient aerodynamic lifting devices.

Three configurations of the Two-Stage-to-Orbit vehicle were proposed for research. The first proposal was to put the orbiter on the bottom or even inside the booster. The second was to take a more radical approach to the problem of orbiter location and place the orbiter on the front of the booster vehicle. The third and final proposal was to take a more conventional approach and place it on the top of the booster. These proposals had their advantages and disadvantages and were given equal consideration.

The bottom mounting would simplify separation problems with the orbiter being basically dropped from the booster. However, a larger vehicle would result and the landing gear system would be complicated. The propulsion system would also be split up, reducing the inlet efficiencies. This proposal was rejected. The orbiter position on the front of the booster would enable its wing to provide some lifting force in the ascent. This would result in a reduced weight for the booster due to the smaller wing area required because the booster would not have to support the entire weight of the vehicle. With the orbiter positioned on the top, minimal contribution could be made to the total vehicle lift. However, the front-mounted orbiter would have a forward-moving center of gravity and would become excessively stable as the flight progressed. This would result in large trim drags. Also, the front-mounted orbiter would complicate landing gear design and also would complicate the separation procedures. The vehicle stability at separation would change dramatically, with a large rearward shift in the center of gravity. This could result in an instantaneous instabilty at separation and would require very large pitching control surfaces and fast, powerful actuators.

The front-mounted orbiter was rejected in favor of the more conventional "piggy-back" design. This design was then developed in more detail for the final conceptual design proposal.

BOOSTER DESIGN

Aerodynamics

Configuration. An overall booster-orbiter gross takeoff weight was determined through a series of size iterations to be 1,112,000 lb. The booster was to make up 820,000 lb of the total weight, with the orbiter taking up the remaining 300,000 lb. A wing loading of 84 lb per sq ft at takeoff was selected to give adequate takeoff performance without the need for auxiliary propulsion takeoff devices. An overall tailless delta configuration was chosen in order to reduce drag at high Mach numbers. The wing was configured as a double-delta planform, with the leading edge swept at 79°-60°. The initial 79° sweep was essentially a leading edge extension (LEX) designed to produce a pitch-up moment to help compensate for the rearward shift of the aerodynamic center as the vehicle passes from subsonic to supersonic flight. The LEX would also reduce the requirement for wing elevons to produce a downward force to maintain static stability.

All-moving tailplanes are located on the wing-tips. The purpose of the tailplanes is to minimize the decrease in lift associated with aft-mounted elevon controls on tailless delta configurations. They also increase the effectiveness of longitudinal control at low speeds and especially at takeoff, where the aircraft must be pitched to an angle of attack for a high lift coefficient. The

all-moving tailplanes were hinged at the trailing edge to increase their lift coefficients. At high speeds, when the required lift coefficient is small and where aileron reversal becomes a problem, the tailplanes are locked out and longitudinal control is taken over by the elevons. This would give the main wing a cranked-arrow type configuration resulting in better efficiency.

To minimize the effect of the elevon with the wing flow field, the directional control surfaces were placed between the wing and the tailplanes. This location gave an endplate-type effect and increased the effective aspect ratio (Fig. 1).

The fuselage was designed with an overall fineness ratio of 7.5. The fuselage was "coke-bottled" to decrease wave drag. The overall length of the booster vehicle was 303 ft with a wingspan of 218 ft (Fig. 2).

Airfoil design. The airfoil section of the booster was specially designed for this project for low wave drag, low heating load, and adequate longitudinal control at high speeds. Two proposals for airfoil sections were designed with the main difference in the leading edge radius. The first had a sharp leading edge to decrease wave drag. The second had a radius/chord ratio of 0.0083 (Fig. 3).

This blunt leading edge reduced the lift-to-drag ratios by approximately 50%. However, no active cooling would be used, and it did have adequate aerodynamic characteristics (Figs. 4 and 5). All supersonic aerodynamic calculations were done using a linearized flow technique.

Computational fluid dynamics method. A linearized flow technique was used to calculate the wing aerodynamic characteristics. Due to the formation of shock waves, the linearized flow technique could not be used at Mach numbers close to 1. The linearized flow model was used in a computer program that required the geometry to be entered in (Fig. 6). The program calculates total lift and drag on the wing by summing up the section lifts and drags by using similar airfoil sections. It calculates the lift and drag on an airfoil section of unit depth starting at the exposed root chord. It then uses a linear model to determine the new airfoil parameters. The planform of the wing must be entered into the program. A linear wing twist model is also incorporated.

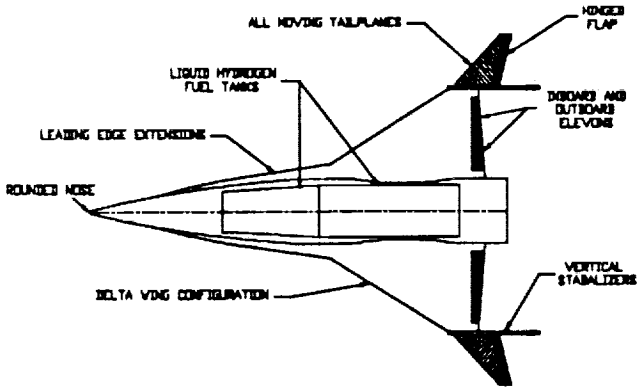

Fig. 1. Key design features.

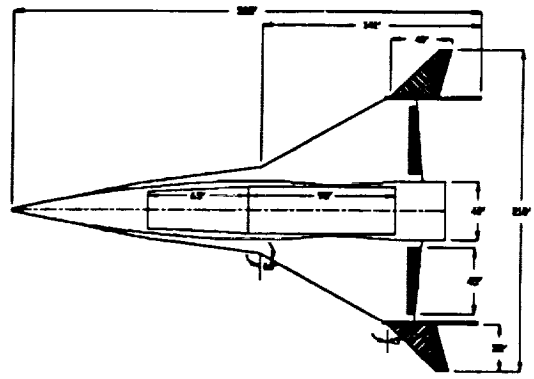

Aircraft Specifications

Aspect Ratio	1.8
S ref	13,320 sq ft
S exp	750 sq ft
S lex	830 sq ft
S tailplane	630 sq ft each
Sweep le	60°
Sweep te	-5°
Taper Ratio	13%
Sweep Tailplane le	45°
Sweep Tailplane te	14°
Taper Ratio Tail	25%

Fig. 2. Booster planform view.

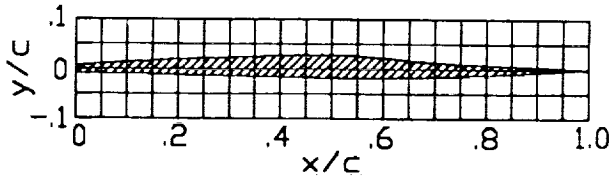

Specifications
Maximum thickness/chord ratio - 0.04 @ x/c = 0.5
Leading edge radius/chord ratio - 0.0083
Positive camber

Fig. 3. Airfoil section proposal number 2.

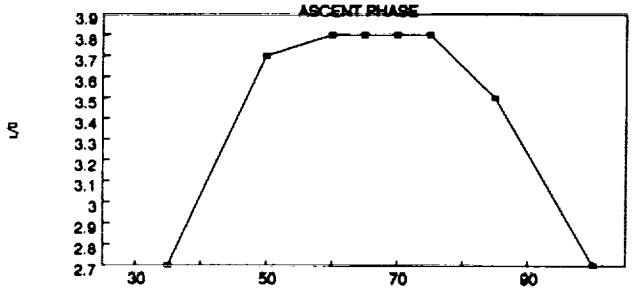

Fig. 4. Lit-to-drag ratio vs. altitude in thousands.

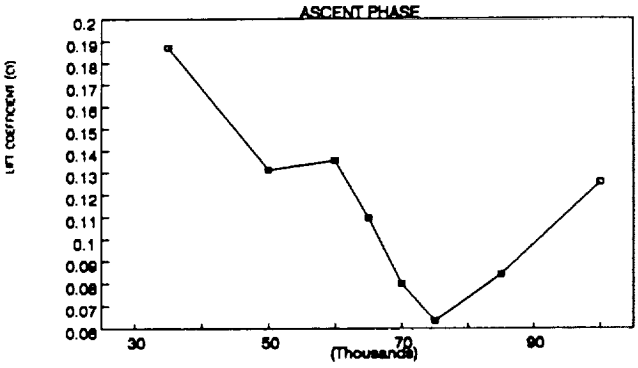

Fig. 5. Lift coefficient vs. altitude in thousands.

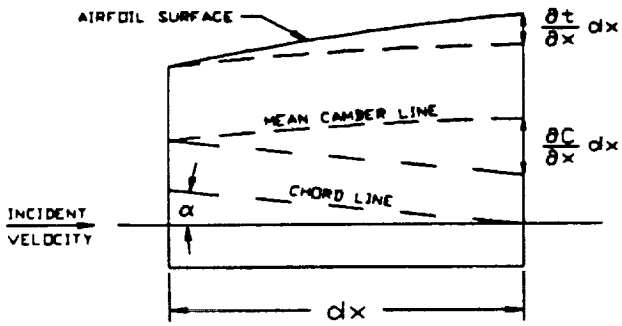

Fig. 6. Surface model used in linearized flow program.

Propulsion

Trajectory analysis. The first consideration in the design of the propulsion system was to compute the trajectory of the booster. This was done by using the energy method. The energy method consisted of generating various curves and then analyzing them to obtain the most efficient flight path. These curves consisted of specific energy heights, specific fuel consumption contours, and a structural limit curve. A minimum fuel-to-climb analysis was then performed. This was accomplished by connecting the points of tangency of the energy heights and the fuel consumption curves, while remaining below the structural limit. For low Mach numbers, this strategy does not apply due to the fact that the curves are essentially perpendicular. Therefore, the aircraft will fly at relatively low altitudes until it reaches approximately Mach 0.8. At this point, the vehicle will climb to approximately 35,000 ft while remaining subsonic. At this point, the vehicle will perform what is sometimes referred to as a "transonic fall." The aircraft literally begins to fall or dive. This is advantageous in two ways. First the fall accelerates the vehicle through the transonic region and second, it requires no additional fuel to perform the maneuver.

After surpassing the transonic region, the minimum fuel-to-climb approach was peformed. Near Mach 2.0 and beyond, the points of tangency of the two curves lie approximately along the structural limit. Therefore, what was done was to follow a path that moved along the structural limit, but with a safety margin of 5000 ft at any point. The vehicle will follow this path and continue to accelerate up to Mach 6.5 at an altitude of 68,000 ft. At this point the vehicle would simply trade a portion of its kinetic energy for potential energy and quickly climb to the required 100,000 ft with no additional power required from the engines.

Boundary layer considerations. The beginning of the inlet is located 162 ft from the nose of the vehicle. At low Mach numbers the boundary layer that is built up from the forebody can be quite substantial. In light of this fact, boundary-layer thickness was calculated and subsequently graphed as a function of Mach number. The results revealed that the boundary-layer thickness ranged from 1.75 ft at subsonic speeds to 1.25 ft at supersonic speeds. A channel-type boundary-layer diverter was selected as a remedy to this problem. This method entails shifting, or in this case, lowering the propulsion system a certain calculated height. The diverter consists of two components. First, a diverter ramp, essentially a wedge, channels the flow around the inlet. In addition to the ramp, a splitter plate extends beyond the start of the diverter ramp to ensure that none of the boundary layer's outer edge is spilled into the inlet.

With this method of boundary-layer removal, the design is assured of strictly high-energy flow entering the turbojet for its full operation time. As for the ramjet, any excess boundary layer that might form can be funnelled through the turbojet. However, at higher Mach numbers, the boundary-layer thickness becomes smaller, so the channel-type diverter should suffice.

Engine selection. An over/under turboramjet with liquid hydrogen fuel was the engine of choice for the propulsion system. This engine was the most attractive choice due to its high performance characteristics. The turbojet produces 160,000 lb of static thrust. This was based on an existing turbojet engine scaled to meet the specifications of the mission. Five turbojets were selected based on the minimum thrust required, maximum weight, and size constraints. The engine measures 26 ft long with a maximum diameter of 4.5 ft. The ramjet's cross sectional area is approximately one-third of the turbojet's, measuring 1.5 ft.

Inlet design. The inlet used was a two-dimensional, dual-ramp, variable geometry, mixed compression inlet. Mixed compression was necessary to decelerate the flow and turn the flow back toward the engine compartments. For subsonic flight, the inlet is flat with a normal shock at the throat. As the vehicle accelerates, the inlet will continually change to induce the required oblique shocks. The inlet design Mach number is 6. This is a 7-shock inlet with two main shocks touching the cowl lip and then a series of reflected shocks and finally a normal shock at the throat. The first ramp measures 28 ft long while the second measures 40 ft. Maximum deflection is 2.5° and 3.5° respectively.

Nozzle integration. Once a cycle analysis was done on both the turbojet and the ramjet, and exit Mach numbers were obtained, a calculation of the exit area of the throat was performed. For the turbojet, a converging-diverging, variable geometry, axisymmetric nozzle was chosen. For the ramjet, a nonaxisymmetric, "half" converging-diverging nozzle was selected. Both of these nozzles satisfy the operating conditions of the system throughout the booster's ascent.

Structure

Materials. The booster is designed to achieve a speed of Mach 6 at an altitude of 100,000 ft. This hypersonic speed induces high skin friction on the vehicle. In turn, high temperatures on the order of 1000-2000° are encountered. The highest temperatures on the vehicle will occur at stagnation points. Areas of concern were the leading edges of the wings and the nose. The materials investigated included titanium aluminide, titanium-based metal matrix composites, carbon-carbon composites, ceramic-matrix composites, copper-matrix composites, and beryllium alloys. The final material selection consisted of titanium aluminide for the skin, a carbon-carbon composite for the nose, and titanium for the understructure.

Weight breakdown. The final weight breakdown of the booster is shown below in Table 1 and Fig. 7. This data includes the gross weight of the orbiter, which will be given in detail in the orbiter section of the report.

TABLE 1. Final weight breakdown of booster

Fuselage	209,361 lb
Wings	230,729
Vertical Tails	22,512
Landing Gear	68,230
Thrust Structure	4,569
Total Structure	535,401 lb
Engines	80,400 lb
Fuel Tank	16,000
Subsystems	40,506
Fuel	160,000
Payload	301,300
GLOW	1,133,000 lb

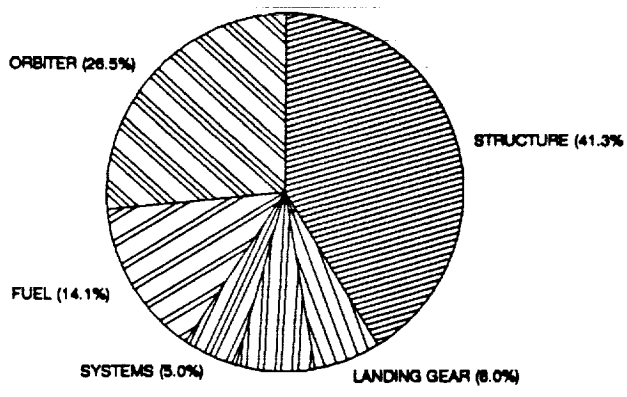

Fig. 7. Booster weight breakdown (takeoff configuration).

ignite its engines to create the first velocity impulse (20,245 ft/s). This impulse will place the orbiter into an elliptical orbit, which will have the 100,000-ft altitude as its perigee.

For the most efficient orbit transfer, the second major velocity impulse will occur at the apogee of the elliptical transfer orbit, which is located at 250 n.m. The velocity impulse (4125 ft/s) will place the orbiter into a circular orbit at this altitude. The timing of the mission must be such that the orbiter and space station rendezvous at approximately this transfer point. In order to allow for a more flexible launch time, the orbiter may be placed in a circular holding orbit, although doing so will increase the necessary amount of fuel.

A third velocity impulse will be required to place the orbiter into the same elliptical transfer orbit so that it can deorbit.

ORBITER DESIGN

Orbiter Trajectory

During the entire trajectory, three major velocity impulses will be necessary. The first major velocity impulse will occur soon after separation from the booster. At the release point, the orbiter will be at 100,000 ft and traveling at Mach 6. At the maximum altitude of the booster's trajectory, the orbiter will be released, and the booster will perform a zero-*g* pushover. Once the booster has reached a safe distance, the orbiter will This final impulse is 4121 ft/s, bringing the total velocity impulse required for the mission to 28,490 ft/s. A diagram showing the various orbits is shown in Fig. 8.

Aerodynamics

Wing design. The initial size estimate for the orbiter wing was based on conditions at landing. Given a lift coefficient of 1.0, a density at sea level of 2.3675E-03 slugs/cu ft, and a landing speed of 300 ft/s, a wing loading of 106.5 lb per sq ft was calculated. Given an initial weight estimate of approximately 90,000 lb, a wing area of 880 sq ft was found. However, if this wing area was implemented, the majority of its surface would lie within the fuselage, leaving very little exposed area for control. Therefore the wing area was increased by approximately 50% to 1200 sq ft. A diagram of the wing, showing all relevant data, is presented in Fig. 9.

The airfoil used for both the wing and tails was designed to withstand the high temperatures encountered during reentry. It was determined that a 6-in leading edge radius would safely withstand the heating values. Therefore, a symmetric airfoil with a 6-in leading edge radius and a maximum thickness-to-chord ratio of 12% was designed.

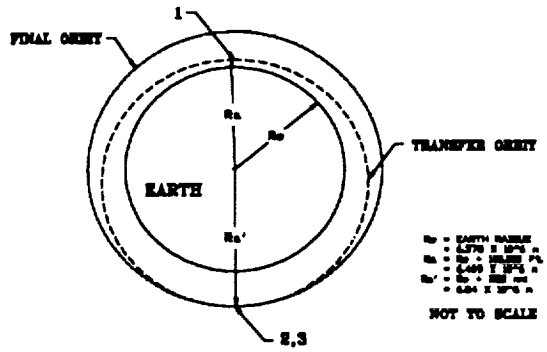

Fig. 8. Orbiter trajectories.

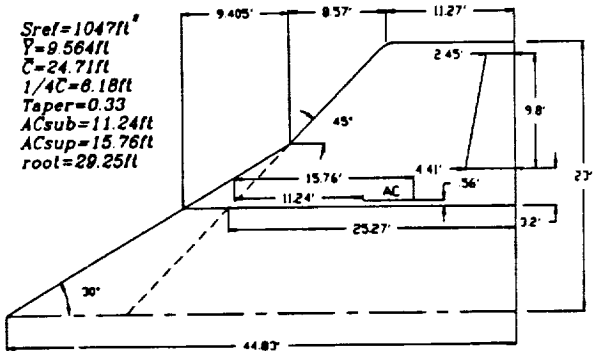

Fig. 9. Wing dimensions.

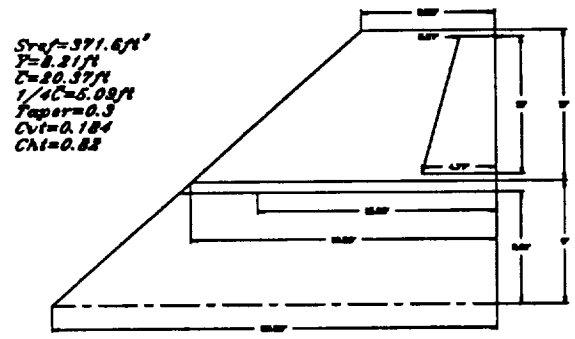

Fig. 10. V-tail dimensions.

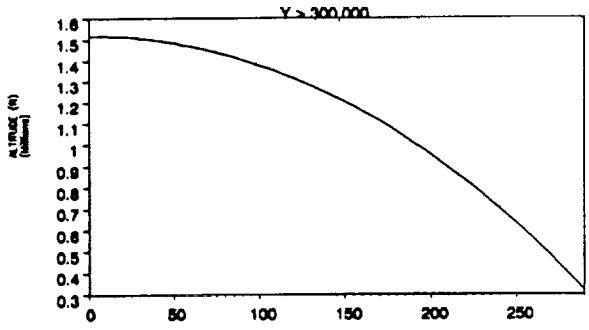

Fig. 11. Orbiter reentry (>300,000 ft vs. time).

Tail design. In an effort to minimize weight, the vertical and horizontal tails were replaced by a V-tail. The V-tail was intended to reduce the wetted area of the tails. With a V-tail, the horizontal and vertical tail forces are the result of horizontal and vertical projections of the force exerted upon the "V" surfaces. In addition, V-tails offer reduced interference drag.

A trapezoid was selected as the basic shape of the V-tail in an attempt to avoid complexity. An 11 ft span from the outer edge of the fuselage was arbitrarily selected and used in the initial calculations. Figure 10 shows a side-view of the V-tail and includes all relevant data pertaining to the V-tail.

Stability and control. Both conditions for static longitudinal stability were met by the orbiter for all four flight regimes: supersonic flight with payload, supersonic flight without payload, subsonic flight with payload, and subsonic flight without payload. The moment coefficient at an absolute angle of attack of 0° is positive provided the angle of attack of the orbiter is positive. Also, the slope of the moment coefficient about the center of gravity is negative for all flight conditions.

The static margins for the various flight regimes differ considerably. The wings were placed on the orbiter so as to provide a minimum static margin of 10%. This occurs when the orbiter is flying subsonically without a payload. However, due to the dramatic shift in the location of the center of gravity when a payload is present, the static margin increases to 50% when the orbiter is flying supersonically and 40% when it is subsonic. These large static margins would produce excessive trim drags which would make it difficult to pilot the orbiter.

Re-entry trajectory. The reentry trajectory from 250 n.m. was calculated in two parts. The first section of the reentry was from orbital altitude to 300,000 ft. At these high altitudes, the atmosphere is so thin that aerodynamic effects are negligible. In the second section, below 300,000 ft, aerodynamic forces are no longer negligible.

Above 300,000 ft, the reentry trajectory was calculated using the equations of motion for a two-body problem. These equations were then integrated to determine the vehicle's position, velocity, and angle of descent as a function of time. A plot of the orbiter's altitude as a function of time is shown in Fig. 11.

Below 300,000 ft, the reentry was determined by aerodynamic forces. The equations of motion were again integrated to determine the altitude, velocity, and angle of descent of the orbiter as a function of time. A check was included to ensure that the deceleration would not exceed 3 *g*. A plot of the orbiter's altitude vs. time for this section is shown in Fig. 12.

Overall, the orbiter's reentry path is similar to that of the shuttle's. However, there are a large number of oscillations present in the data. These oscillations could be dampened with a controller that was too complex to develop in the allotted time period.

Aerodynamic heating. The aerodynamic heating incurred upon atmospheric reentry affects many aspects of the orbiter's design, most importantly, structure weight. The temperatures that occur during a typical reentry require that the windward surfaces of the orbiter be covered with a temperature-resistant material. The available materials can result in a large weight penalty; therefore, the aerothermodynamic environment of the orbiter was carefully considered.

Both temperature and heat transfer rate, along with heat load, were calculated at the orbiter nose and the wing leading edge, two areas of severe heating effects. These quantities are functions of velocity, altitude, material emmissivity, and airframe geometry.

The results of the heating calculations can be seen in Figs. 13 and 14. The maximum heat load that the material can withstand is 70,480 Btu/sq ft. The heat loads for the orbiter's nose and leading edges are both well below this value. While the maximum values of T_w at the nose and leading edges appear excessively high, this is due to the oscillatory nature of the reentry trajectory. If the reentry could be managed more effectively and the oscillations in velocity and altitude could be reduced, the maximum values of T_w would be more

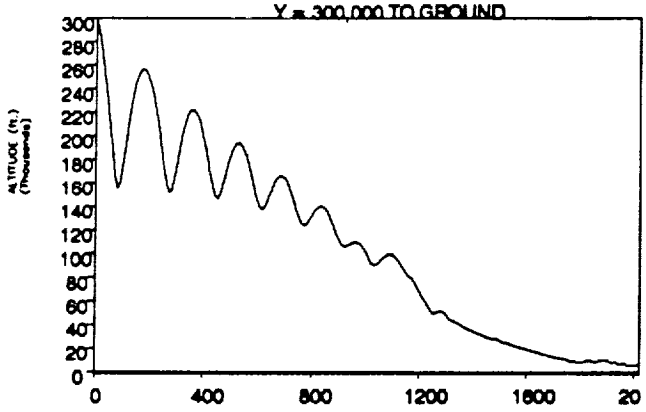

Fig. 12. Orbiter reentry (300,000 ft to ground vs. time).

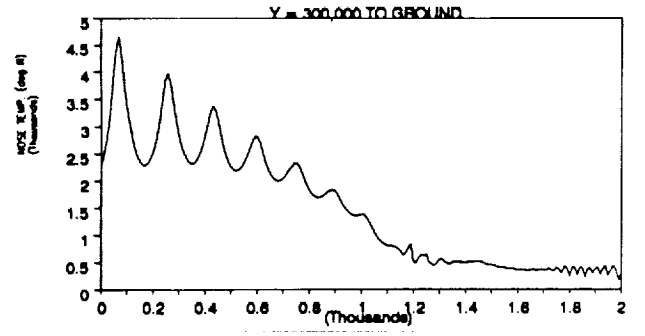

Fig. 13. Orbiter reentry (Nose temperature vs. altitude).

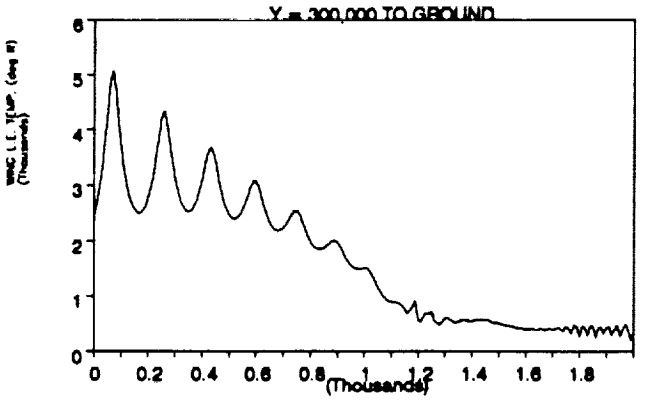

Fig. 14. Orbiter reentry (Leading edge temperatue vs. altitude).

reasonable. Wall temperatures around 3000°F would be possible. This temperature is within the range that materials available in the near future will withstand without severe weight penalty.

Landing performance. The final aerodynamic calculation was to investigate the distance traveled by the orbiter once it touched down. Two landing conditions were considered: landing with a payload and landing without a payload. The first of these yielded a total ground roll of approximately 8600 ft, and the second resulted in a total ground roll of just over 6700 ft. Both of these conditions assume that the orbiter's fuel tanks are empty.

Propulsion

In designing the propulsion system for the orbiter, several performance requirements had to be met. It was of primary importance that the system be sufficient to provide the necessary thrust to obtain orbital velocity and to facilitate orbital transfers. A second requirement was that the vehicle be equipped with control thrusters to allow for translation and rotation in all axes. Encompassing all other requirements was the stipulation that the overall system weight, including propellants, be as low as possible.

The first step taken in the design of the system was to research the available propellants and to choose that primary fuel/oxidizer combination that would best meet the stated requirements. After examining several possible combinations, it was decided to use liquid hydrogen as the fuel and liquid oxygen as the oxidizer. Having selected the propellants, it was then possible to proceed with the design of the system components.

Main engine. The function of the main engine in this vehicle is to provide the necessary thrust to reach orbital velocity from an initial release velocity of 6000 ft/s. It was decided that the main engine would not be used for orbital transfers and thus could be designed specifically for high-thrust, long-duration firing, eliminating major concerns for transient operation and wide throttling requirements. These functional requirements can be met by the "next-generation SSME," which was specified as the main engine. Estimates were then made on the engine's performance based upon recent data and expected advances in materials technology in future years.

Orbital maneuvering engines. The OMEs serve to provide the required thrust for orbital transfers and major maneuvering. Thus the engines must be designed to be restartable and to have controllable thrust vectors for precise maneuvering. Based on the preliminary configuration of the orbiter fuselage, it was decided that a pair of engines, mounted on each side of the main engine would be the most effective configuration. An advantage of this type of mounting is that the maneuvering engines need only be gimballed to obtain pitching moments, since yaw moments can be obtained by simply decreasing the thrust from one of the OMEs. As for fuel, since the hydrogen and oxygen tanks are a permanent part of the vehicle, it was decided that it would be advantageous to design the engines to operate with this fuel/oxidizer combination.

The actual engine design was based primarily on information presented in a paper entitled Advanced LO_2/LH_2 Space Engine Characteristics, published by Rocketdyne. The final design has both engines gimballed for thrust vector control, and the exit plane of the OMEs coinciding with the exit plane of the main engine, to avoid external nozzle damage. A single propellant feed system was chosen with separate flow control valves for each engine to facilitate thrust modulation. A schematic of the mounting scheme can be seen in Fig. 15.

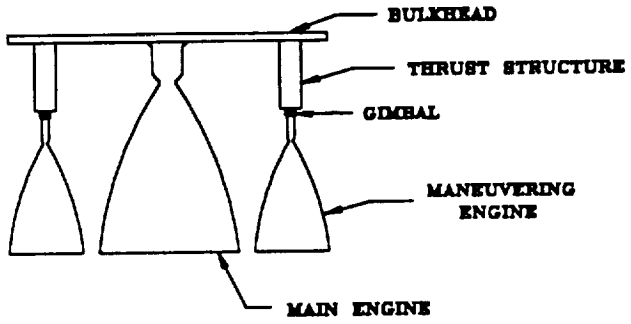

Fig. 15. Orbital engine mounting.

Attitude control rockets. The attitude control rockets have the primary function of controlling the orientation of the vehicle while in space. Thus a main requirement of these rockets is that enough thrust is produced so that maneuvers may be performed within a reasonable time allotment. A second requirement is that each rocket can be restarted thousands of times, and that each burn time be controllable to within a few hundredths of a second, providing precise maneuvering capabilities.

A detailed analysis was performed and it was determined that a minimum of 16 thrusts would be needed, and that a redundant thruster for each required should be included, insuring that no one thruster failure could disable the attitude control system. For fuel, it was decided to use monomethyl hydrazine and nitrogen tetroxide with a gas pressure feed system. Major engine specifications are presented in Table 2.

TABLE 2. Engine specifications

SSME:	
Maximum Thrust	493,000 lb
I_{sp}	493 s
Weight	5362 lb
OME:	
Maximum Thrust	7500 lb (each)
I_{sp}	493 s
Weight	266 lb (each)
Attitude Control Rockets:	
Maximum Thrust	900 lb (each)
I_{sp}	300 s
Weight	30 lb (each)

Structures

Wing design. Once the total area and shape of the wing was determined, it was possible to make estimates of the internal structural layout and the skin thicknesses. A sparswise lift distribution was determined to range from 2081-989 lb at the tip of the wing. These lift calculations were based on area increments from the root to the tip of the wing, using a wing loading of 84 lb/sq ft. The wing weight was estimated to be 4.5 lb/sq ft. The net lift was found by subtracting the incremental wing weight from the lift. From this, the shear force and bending moment distributions were calculated.

The internal structure of the wing consists of three spars. Two spars are load bearing and are located at 0.2 and 0.8 chord lengths from the leading edge. The third spar is smaller and non-load bearing. It is used for lateral support of the ribs. The two load-bearing spars are located on the lower edge of the wing, while the third is on the upper edge. These spars were modeled as I-beams. The leading edge spar is a 12-in I-beam with a flange width of 6 in, a thickness of 0.4375 in, and a web thickness of 0.25 in. The trailing edge spar is tapered from a height of 12 in to 3 in at the tip. It has a flange dimension of 6 in by 0.3125 in and a web thickness of 0.25 in. The center spar has a flange that is 3 in by 0.25 in and a web that is 6 in by 0.25 in. The two load bearing spars are connected by 12-in I-beam carrythroughs. The carrythoughs are fastened to the fuselage frame members as well as the wing fillets.

The ribs are fabricated from a sheet of 1/8-in thick titanium with 70% of the area cut out for weight reduction. Each rib has a 2-in-wide flange around it to facilitate the skin mounting. There are 10 ribs per wing. A schematic of the wing structure is shown in Fig. 16.

Fuselage design. The fuselage is composed of circular frame elements that are connected by a network of 12 stringers placed equally around the circumference of the fuselage. The frame element was designed to fit the size requirements of the tanks, payload area, and outer shell. The frame element consists of a fabricated circular I-beam with a 12-in-high web and a 2-in-wide flange on both sides. Both the web and flanges were constructed from 1/8-in-thick titanium. To minimize weight, we included 24 6-in-diameter cutouts, which are located in pairs between the spars. Figure 17 shows this frame element. These frame members are connected by a series of 12 stringers. These I-beam-shaped members have a 12-in-high web and a 2-in-wide flange, each of which are 1/8-in thick. There are 16 frame members spaced equally along the length of the fuselage. In addition, there are three bulkheads: two are fore and aft of the payload bay and a third serves as the thrust structure to which the engines are mounted.

Thermal protection system. The selection of the thermal protection system was based upon weight, maximum temperature limit, system simplicity, and available information. The

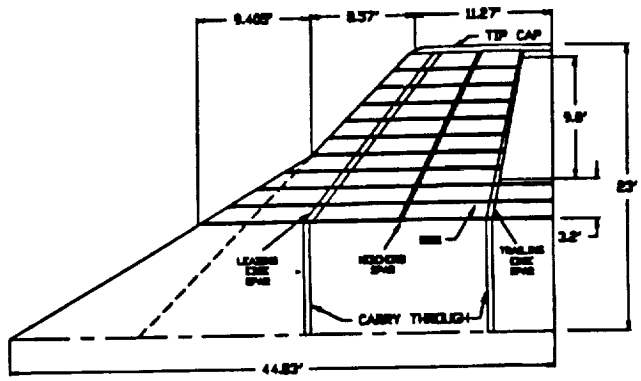

Fig. 16. Wing structure.

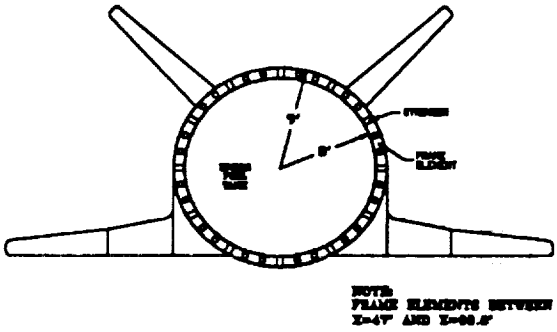

Fig. 17. Structural cross section.

TABLE 3. Orbiter weight breakdown (lb)

Wings	4,985
Wing (TPS)	2,740
V-Tail	1,500
V-Tail (TPS)	529
Fuselage	10,063
Fuselage (TPS)	9,203
Nose	3,000
Nose (TPS)	2,510
Nose Gear	1,000
Main Gear	4,000
LOX Tank	1,634
LH_2 Tank	3,811
N_2O_4 Tank	50
MMH Tank	43
Total Structure	45,067
Total TPS Weight	14,982
Propulsion Group	
Main Engine	5,362
OMEs	532
Total	5,894
Subsystems	
Control	10,000
Hydraulic	5,000
Crew Compartment	4,280
Total	19,280
Total Empty Weight	70,241
Maximum Payload	20,000
Fuel Weights	
LOX	179,600
LH_2	29,930
N_2O_4	1,010
MMH	490
Total	211,030
Gross Weight	301,271

Fiber-Fiber Rigid Composite Insulation (FRCI) system was selected. FRCI is a ceramic composite silica and aluminaborosilicate fiber. This serves as the insulation layer.

A coating of RCG is applied to the FRCI insulation to protect it from aerodynamic stresses. Polymide graphite was selected as the structural skin of the orbiter. It has an operational temperature limit of over 500°F and is very lightweight. The insulation tiles are glued to the polymide graphite skin with RTV 560, a high-temperature adhesive. A final weight breakdown of the orbiter can be found in Table 3 and Fig. 18 along with a two-view of the orbiter in Fig. 19.

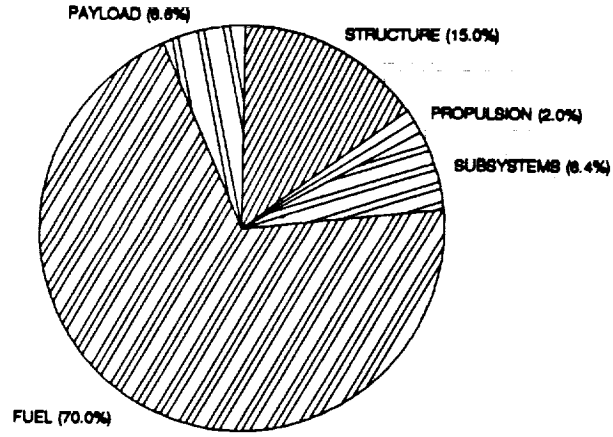

Fig. 18. Weight breakdown at gross takeoff weight.

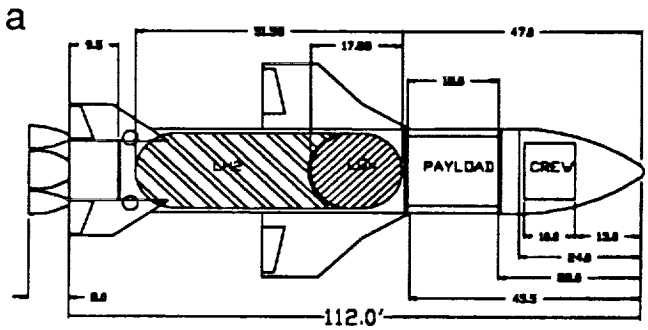

Fig. 19. (a) Orbiter top view.

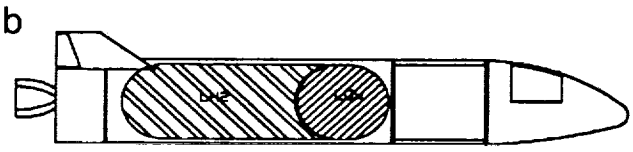

(b) Orbiter side view.

CONCLUSION

The final design is presented in Fig. 20. This conceptual design has the following three advantages over the space shuttle. First, the use of high specific impulse air-breathing engines during its initial ascent reduces the mission's fuel requirements and thus the cost of placing the payload into orbit. Second, unlike the space shuttle, this vehicle was designed to be completely reusable, thereby further reducing its cost by eliminating the need for substantial refurbishment after each mission. Third, due to the reduction in turnaround time, NASA's profitability would increase both in absolute and in per unit terms by expanding the capacity to launch more missions per year and reducing the cost of each as well.

Unlike proposed single-stage-to-orbit vehicles, the orbiter of this design does not have the added weight of air-breathing engines to carry into space. This reduces the fuel requirement, thereby further reducing the cost of each mission. This conceptual design of a two-stage-to-orbit vehicle appears to be a viable option for the next-generation space shuttle.

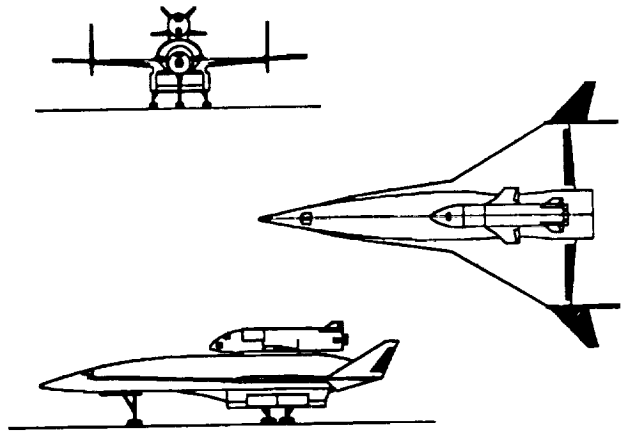

Fig. 20. Final design of two-stage-to-orbit vehicle.